Numerical Analysis on Two Floating Offshore Wind Turbines with Different Layouts

***Yang Huang, Ping Cheng and †Decheng Wan**

Collaborative Innovation Center for Advanced Ship and Deep-Sea Exploration, State Key Laboratory of Ocean Engineering, School of Naval Architecture, Ocean and Civil Engineering, Shanghai Jiao Tong University, Shanghai, China

*Presenting author: 958185119@qq.com
†Corresponding author: dcwan@sjtu.edu.cn

Abstract

The layout of wind turbines has significant effects on the power generating capacity and the economic efficiency of the wind farm. How to rationally arrange the wind turbines, minimize the mutual interference in the wake, and improve the efficiency of the whole wind farm have been paid enough attention. To investigate the aero-hydrodynamic characteristics of floating offshore wind turbines (FOWTs) with different layouts, fully coupled simulations for FOWTs under variable wind and wave conditions are necessary. In the present work, the unsteady actuator line model (UALM) is embedded into in-house CFD solver naoe-FOAM-SJTU to establish a fully coupled CFD analysis tool named FOWT-UALM-SJTU for numerical simulations of FOWTs. Coupled aero-hydrodynamic simulations of two OC3 Hywindspar FOWT models in both tandem and offset configurations under shear wind and regular wave conditions are performed. From the simulations, unsteady aerodynamic characteristics including the rotor power, thrust, and detailed wake flow information can be obtained, and hydrodynamic responses such as the six-degree-of-freedom motions and mooring tensions are also available. The coupled aero-hydrodynamic characteristics of FOWTs with different layouts are compared and analyzed. Strong wake interaction phenomena are observed and the blades of the downstream turbine are subject to a highly asymmetric interaction with the wake induced by the upstream turbine in offset configuration. The coupled aero-hydrodynamic performance of downstream FOWT is significant influenced by the layout of FOWTs.

Keywords: **Floating offshore wind turbines; Coupled aero-hydrodynamic simulations; Layout of wind turbines; FOWT-UALM-SJTU solver**

Introduction

Along with the growing energy crisis and environmental crisis, the demands of renewable energy have become increasing urgent. As one of the most promising non-polluting renewable energy, wind energy is developing rapidly in recent years. In addition, the wind turbines that are used to convert the wind energy into electricity have also achieved great development. To obtain more wind power, the rotor blade of wind turbines have become significant larger. The wind turbine sizes have increased to multi-megawatt levels. Additionally, the wind turbine have experienced from onshore wind turbines to offshore wind turbines for gaining huge amount wind energy. Compared with onshore wind turbines, the offshore wind turbines have several advantages. The wind speed from the sea is much stronger and more uniform than it from the land, which means the offshore wind turbines can again more wind energy than onshore wind turbines. The onshore wind turbines have constraints such as visual impact and noise emissions, while the onshore wind turbines can avoid these disadvantages and do not take up precious land resources[1]. The using of offshore wind turbines has become a trend in the development of wind energy, and the offshore wind farms composed of multiple offshore wind turbines for the development of huge amount offshore wind power have attracted a lot of attention.

In the offshore wind farms, the layout design has great influence on the initial investment cost, annual energy production, operation and maintenance cost during the service life time of wind turbines[2]. An adequate wind farm layout design would lead to higher than expected wind power capture, decreased maintenance costs, longer service time, and so on. Many research works focusing on the layout design have been done. Bansal et al.[3] improved the biogeography based optimization (BBO) and solved the wind farm layout optimization problem with non-uniform hub height and rotor radius based on fitness difference strategy (FD-BBO). Compared with numerical experiments on benchmark test problems, the proposed FD-BBO was proven to be an efficient optimization algorithm. Wang et al.[4] presented a novel control strategy approach for the optimization of a simple square wind farm, and optimal wind farm design considering both the wind turbine placement and control were studied using three different optimization approaches. Rehman et al.[5] proposed an optimization approach based on the cuckoo search (CS) algorithm for wind farm layout design. The proposed CS algorithms were compared with genetic and particle swarm optimization algorithms, and the comparative results including the yearly power output and efficiency showed the CS algorithms outperformed other optimization algorithms. Choi et al.[6][7] performed numerical simulations of a 6 MW wind farm consisting of three sets of 2MW wind turbines in tandem configutation. The influence of the inter-turbine spacing on the aerodynamic power output, wake interaction and the dynamic responses of wind turbine was studied. They also investigated the aerodynamic performance of a wind farm with two sets of 2MW class wind turbines using a full 3-D wind turbine model. The effect of separation distance between two turbines on power output of the wind farm was studied. Fletcher and Brown[8] studied the aerodynamic interaction between two wind turbines in both co-axial and offset configurations using vorticity transport model. The influence of horizontal space and longitudinal space on the aerodynamic interaction was discussed. Mikkelsen et al.[9] analyzed the effect of wake interaction for three in-line model wind turbines in a wind farm based on the actuator line technique. Both full wake and half wake situations are considered, and detailed unsteady behavior of interacting wakes was captured.

With the progress in offshore wind energy, the floating wind farms are planned for huge amount of clean electricity recently. The floating offshore wind turbines (FOWTs) are usually clustered in the floating wind farms to decrease the overall installation and maintenance expenses, causing an adverse effect that the wind turbines generally experience a significant increased turbulence because of wake interaction from surrounding wind turbines[10]. Considering the fact that the wake interaction between FOWTs has remarkable effects on the FOWT's power output, system dynamic responses and structural loadings, it should be paid enough attention. The wake interaction phenomena is observed and investigated originally in onshore wind farms, and many researches have been conducted to study the influence of complicated wake characteristics on wind turbines in onshore wind farms. Initially, different wake field models[11]-[14] are developed for the wake calculations. But detailed turbulence characteristics in the wake flow, which have great influence on wake interaction, cannot be obtained. To better understand the complicated wake characteristics in wind farms, model tests[15][16] are also conducted. The wake characteristics of wind turbines and the wake interaction phenomena are investigated based on wind tunnel tests. Considering the influence of scale effect on wake flow cannot be avoided in the model tests, CFD techniques that can consider turbulence characteristics in wake flow and eliminate the influence of scale effect become more and more popular in the study of wake interaction in wind farms. Churchfield et al.[17] investigated the influence of atmospheric stability and surface roughness on wind turbine dynamics. Numerical simulations for two wind turbines were conducted to study the wake effects under different surface roughness and atmosphere conditions. Troldborg et al.[18] studied the wake interaction between two wind turbines based on the actuator line model. Different ambient turbulence intensities were taken into consideration in the simulations. The averaged velocity and turbulence fields as well as the development of wake generated vortex structure were extracted to understand the interacting wakes. For floating wind farms, the environment loads acting on the FOWTs are complex, and the coupling effects between wind turbine and floating platform make the wake interaction more complicated. Dörenkämper et al.[19] studied the impact of the stratified atmospheric boundary layer on power production and wake effects in offshore wind farms by the means of measurements large-eddy simulations. Barthelmie et al.[20] modelled the wake of large wind farms based on computational fluid dynamics models and analyzed the power losses due to wakes at offshore wind farms. Above all, far limited work have been done to investigate the complicated wake field characteristics in floating wind farms. It is necessary to study coupled aero-hydrodynamic responses of FOWTs and wake flow filed in floating wind farms for optimal layout design.

In the present paper, the unsteady actuator line model (UALM) is embedded into in-house CFD solver naoe-FOAM-SJTU to establish a fully coupled CFD analysis tool named FOWT-UALM-SJTU for full-scale simulations of FOWTs. Coupled aero-hydrodynamic simulations of two OC3 Hywindspar FOWT models in both tandem and offset configurations under shear wind and regular wave conditions are performed. From the simulations, unsteady aerodynamic characteristics including the rotor power, thrust, and detailed wake flow information can be obtained, and hydrodynamic responses such as the six-degree-of-freedom motions and mooring tensions are also available. The coupled aero-hydrodynamic characteristics of FOWTs with different layouts are compared and analyzed to study the influence of layout of FOWTs.

Numerical Method

The Unsteady Actuator Line Model

The actuator line model (ALM) developed by Sørensen and Shen[21] is a simplified method to study the aerodynamic performance of wind turbine. It is an effective way to displace the real tower surfaces with virtual actuator lines. In consequence, it acquires a benefit of not requiring to solve the blade geometry layer. The body forces distributed along the lines are calculated from the local attack angle and a look-up table of airfoil data. The main advantage of modeling the rotor of wind turbine using ALM is that the calculation resource can be greatly saved.

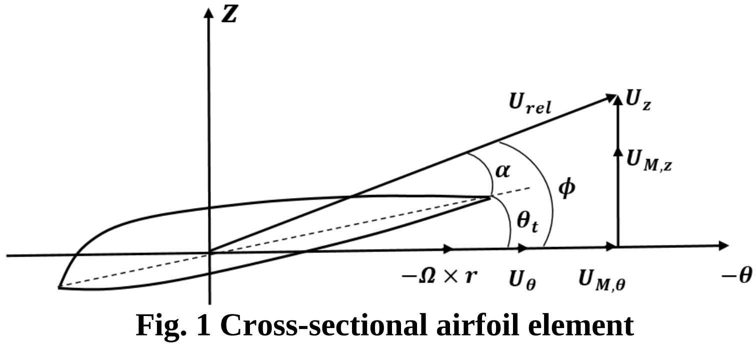

Fig. 1 Cross-sectional airfoil element

In the present work, modifications should be made to the initial ALM so that it can be used to simulate the FOWT. This is accomplished by accounting for the influence of the platform

motion ($\boldsymbol{U_M}$ shown in Fig. 1) on the blades. Then the UALM used in this study is developed by modifying the initial ALM. To determine the body forces acting on the blades, a blade element approach combined with two-dimensional airfoil characteristics is used. As Fig. 1 shows, a cross-sectional element at radius r defines the airfoil at the (θ, z) plane. Denoting the tangential and axial velocity in the inertial frame of reference as $\boldsymbol{U_\theta}$ and $\boldsymbol{U_z}$, respectively. $\boldsymbol{U_M}$ represents the added velocity vector induced by the motions of floating support platform, which will lead to complicated interactions between the rotor and its wake.
The integral velocity vector relationship can be described as:

$$\boldsymbol{U}_{rel} = \boldsymbol{U}_\theta - \boldsymbol{\Omega} \times \boldsymbol{r} + \boldsymbol{U}_z + \boldsymbol{U}_M \tag{1}$$

Where Ω is the angular velocity of the rotor. The local velocity U_{rel} relative to the rotating blade is calculated as:

$$|U_{rel}| = \sqrt{(U_z + U_{M,z})^2 + (U_\theta - \Omega r + U_{M,\theta})^2} \tag{2}$$

Here $U_{M,\theta}$ and $U_{M,Z}$ are the projections of $\boldsymbol{U}_M$ on (θ, z) plane.
The attack angle is defined as:

$$\alpha = \phi - \theta_t \tag{3}$$

Where $\phi = \tan^{-1}\left(\frac{U_z + U_{M,z}}{U_\theta - \Omega r + U_{M,\theta}}\right)$ is the inflow angle. θ_t is the local twist angle. And the body force can be given by the following equation:

$$\boldsymbol{f} = (\boldsymbol{L}, \boldsymbol{D}) = \frac{\rho |U_{rel}|^2 c N_b}{2 r d\theta dz}(C_L \boldsymbol{e}_L + C_D \boldsymbol{e}_D) \tag{4}$$

Where c is the chord length; N_b is the number of blades; C_L and C_D are the lift and drag coefficient, respectively; $\boldsymbol{e}_L$ and $\boldsymbol{e}_D$ denote the unit vectors in the directions of the lift and the drag, respectively. The lift and drag coefficients are determined from measured or computed two-dimensional airfoil data that are corrected for three-dimensional effects.
The body force needs to be smoothed to avoid singular behavior before it is added into the momentum equations.

$$\boldsymbol{f}_\varepsilon = \boldsymbol{f} \otimes \eta_\varepsilon \tag{5}$$

where

$$\eta_\varepsilon(d) = \frac{1}{\varepsilon^3 \pi^{3/2}} exp\left[-\left(\frac{d}{\varepsilon}\right)^2\right] \tag{6}$$

Here d is the distance between the measured point and the initial force points on the rotor. ε is a constant which serves to adjust the strength of regularization function, and the influence of the parameter ε has been studied and some experienced conclusions have been obtained[22].
The regularized force pre unit volume force can be written as:

$$\boldsymbol{f}_\varepsilon(\boldsymbol{x}, \boldsymbol{y}, \boldsymbol{z}, \boldsymbol{t}) = \sum_{i=1}^{N} \boldsymbol{f}(\boldsymbol{x}_i, \boldsymbol{y}_i, \boldsymbol{z}_i, \boldsymbol{t}) \frac{\mathbf{1}}{\boldsymbol{\varepsilon}^3 \boldsymbol{\pi}^{3/2}} \boldsymbol{exp}\left[-\left(\frac{\boldsymbol{d}}{\boldsymbol{\varepsilon}}\right)^{\mathbf{2}}\right] \tag{7}$$

Then $\boldsymbol{f}_\varepsilon$ is added into the right hand of momentum equations as a source term.

Six-degree-of-freedom Motions

The six-degree-of-freedom motions of the floating support platform are predicted by in-house CFD solver naoe-FOAM-SJTU. Two coordinate systems (as shown in Fig. 2) are used in the procedure of solving six-degree-of-freedom motion equations. In each time step simulation, the motion equations are solved in platform-fixed coordinate system and the forces are calculated in earth-fixed coordinate system. And the added velocity induced by the motions of floating support platform is updated by the following equation:

$$\boldsymbol{U}_{M,i} = [\boldsymbol{J}](\boldsymbol{U}_c + \boldsymbol{\omega}_c \cdot (x_i - x_c)) \tag{8}$$

Where $[\boldsymbol{J}]$ is the transformation matrix defined from the platform-fixed coordinate to earth-fixed coordinate; $\boldsymbol{U}_c$ and $\boldsymbol{\omega}_c$ donate the translation velocity and the angular velocity of the rotating center, respectively; x_c is the position coordinate of the rotating center.

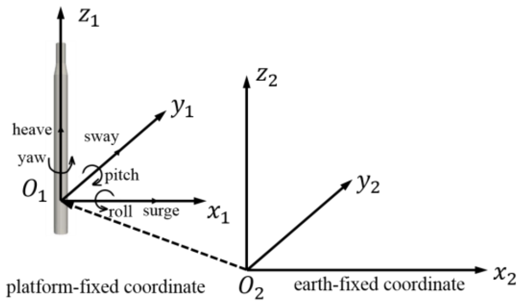

Fig. 2 Two coordinate systems

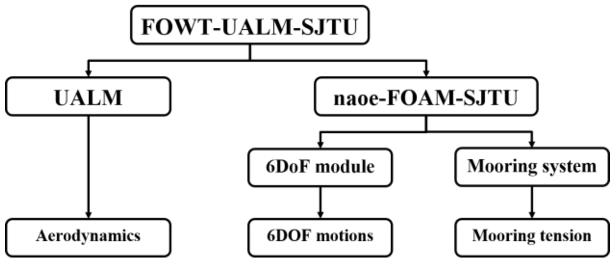

Fig. 3 Frame diagram of FOWT-UALM-SJTU

Coupled Aero-hydrodynamic Analysis Method

In the present work, the UALM is embedded into naoe-FOAM-SJTU to establish a fully coupled CFD analysis tool named FOWT-UALM-SJTU to study the coupled aero-hydrodynamic characteristics of FOWTs. As Fig. 3 shows, the aerodynamic forces can be got by the UALM, and the six-degree-of-freedom motions are predicted by the naoe-FOAM-SJTU. Moreover, the piecewise extrapolating method (PEM) is used to study the performance of the mooring system. It is static analysis method. The gravity and tensile deformation of mooring lines are both taken into consideration in the calculation of mooring tensions.

In FOWT-UALM-SJTU solver, VOF (Volume of Fluid) method with bounded compression technique is used to solve two-phase flow problem with free surface. The *k*-*ω* SST turbulence model is applied to solve the RANS equation. And the governing equations can be written as:

$$\nabla \cdot \boldsymbol{U} = 0 \tag{9}$$

$$\frac{\partial \rho \boldsymbol{U}}{\partial t} + \nabla \cdot \left(\rho\left(\boldsymbol{U} - \boldsymbol{U}_g\right)\right)\boldsymbol{U} = -\nabla p_d - \boldsymbol{g} \cdot x \nabla \rho + \nabla \cdot \left(\mu_{eff} \nabla \boldsymbol{U}\right) + (\nabla \boldsymbol{U}) \cdot \nabla \mu_{eff} + \boldsymbol{f}_\sigma + \boldsymbol{f}_s + \boldsymbol{f}_\varepsilon \tag{10}$$

Where $\boldsymbol{U}$ is velocity of field; $\boldsymbol{U}_g$ is the velocity of mesh points; $p_d = p - \rho \boldsymbol{g} \cdot x$ is the dynamic pressure, subtracting hydrostatic component from total pressure; $\boldsymbol{g}$ is the gravity of acceleration vector; ρ is the mixture density with two phases; $\mu_{eff} = \rho(\nu + \nu_t)$ is effective dynamic viscosity, in which ν and ν_t are kinematic viscosity and eddy viscosity respectively; $\boldsymbol{f}_\sigma$ is the surface tension term in two phases model and takes effect only on the liquid free surface; $\boldsymbol{f}_s$ is the source term for sponge layer, which is set to avoid the wave reflection at the end of the tank and takes effect only in sponge layer; $\boldsymbol{f}_\varepsilon$ is the body force calculated from UALM, representing the effects of turbine blades on the flow field.

The solving procedure of coupled aero-hydrodynamic simulations for the FOWTs is shown in Fig. 4. Coupling effects between the wind turbine, floating platform and mooring system are considered. It can be found that the calculated motion responses are inputs of UALM. The calculation of body force needs the information of the motions of the floating platform. In addition, the calculated aerodynamic forces are also inputs of the calculation of six-degree-of-freedom (6DoF) motions. It can be seen that the aerodynamic forces obtained from the UALM are added into the 6DoF motion equations.

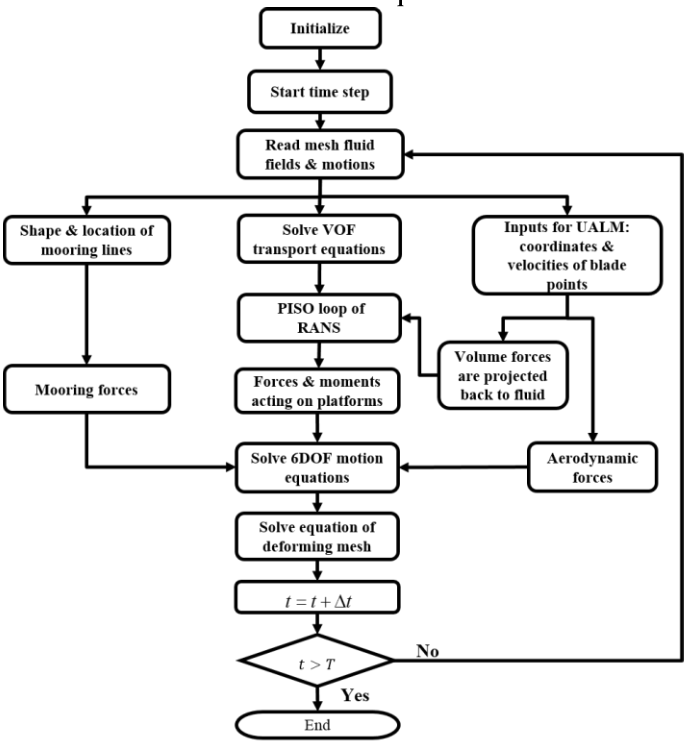

Fig. 4 Solving procedure of coupled aero-hydrodynamic simulations

Simulation Conditions

Geometric Model

The FOWT model used in the present work is OC3 Hywindspar FOWT model. General arrangement of the FWOT system is shown in Fig. 5. The wind turbine is NERL offshore 5-MV baseline wind turbine, which is a conventional three-bladed, upwind, variable-speed and variable blade-pitch-to-feather controlled turbine. The main specifications of the wind turbine are given in Table 1[23].

Table 1 Specifications of NERL 5-MW turbine

Rating	5 MW
Rotor Orientation, Configuration	Upwind, 3 Blades
Control	Variable Speed, Collective Pitch
Drivetrain	High Speed, Multiple-Stage Gearbox
Rotor, Hub Diameter	126 m, 3 m
Hub Height	90 m
Cut-in, Rated, Cut-out Wind Speed	3 m/s, 11.4 m/s, 25 m/s
Cut-in, Rated Rotor Speed	6.9 rpm, 12.1 rpm
Rated Tip Speed	80 m/s
Overhang, Shaft Tilt, Precone Angle	5 m, 5°, 2.5°
Rotor Mass	110,000 kg

Nacelle Mass	240,000 kg
Tower Mass	347,460 kg
Coordinate Location of Overall Center of Mass	(-0.2 m, 0.0 m, 64.0 m)

The floating support platform is the spar-buoy concept platform called Hywindspar applied in OC3 project, and detailed information is listed in Table 2[24].

Table 2 Specifications of Hywindspar platform

Depth to Platform Base Below SWL (Total Draft)	120 m
Elevation to Platform Top (Tower Base) Above SWL	10 m
Depth to Top of Taper Below SWL	4 m
Depth to Bottom of Taper Below SWL	12 m
Platform Diameter Above Taper	6.5 m
Platform Diameter Below Taper	9.4 m
Platform Mass, Including Ballast	7,466,330 kg
CML Location Below SWL Along Platform Center Line	89.9155 m
Platform Roll Inertia about CM	4,229,230,000 kg•m^2
Platform Pitch Inertia about CM	4,229,230,000 kg•m^2
Platform Yaw Inertia about Platform Centerline	164,230,000 kg•m^2

The mooring system consisting of three mooring lines is symmetrically distributed around the platform. Main characteristics of the mooring system are shown in Table 3. And the arrangement of the mooring lines is shown in Fig. 6.

Table 3 Parameters of mooring system for OC3-HywindSpar platform

Number of Mooring Lines	3
Angle Between Adjacent Lines	120°
Depth to Anchors Below SWL (water depth)	320 m
Depth to Fairleads Below SWL	70.0 m
Radius to Anchors From Platform Centerline	853.87 m
Radius to Fairleads From Platform Centerline	5.2 m
Unstretched Mooring line length	902.2 m
Mooring Line Diameter	0.09 m
Equivalent Mooring Line Mass Density	77.7066 kg/m
Equivalent Mooring Line Mass Weight in Water	689.094 N/m
Equivalent Mooring Line Extensional Stiffness	384,243,000 N
Additional Yaw Spring Stiffness	98,340,000 Nm/rad

Fig.5 Sketch of FOWT system

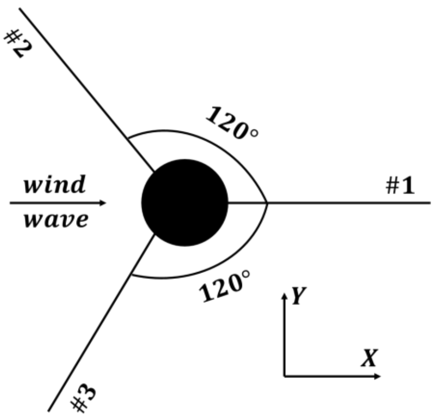

Fig. 6 Mooring system

Simulation Conditions

To investigate the aero-hydrodynamic characteristics of FOWTs with different layouts, fully coupled simulations for FOWTs under variable wind and wave conditions are performed. In this work, coupled aero-hydrodynamic simulations of two OC3 Hywindspar FOWT models in both tandem and offset configurations under shear wind and regular wave conditions are conducted. Detailed simulation cases are listed in Table 4.

Wind and wave conditions are kept in the same in these two cases. Wave period and wave length are T = 10s and λ = 156m, respectively. And the wave height is H = 4m. Considering the characteristics of height-dependent wind speed, exponential model is used to describe wind shear.

$$u_Z = u_0 \times \left(\frac{z}{90}\right)^{0.143} \tag{11}$$

Where u_Z is the wind velocity at the height of z, u_0 is the wind velocity at the height of hub center. And the wind speed in these case are kept in the same at u_0 = 5 m/s.

Table 4 Simulation cases

Case Number	Distance along *x* direction	Distance along *y* direction
Case 1 (tandem case)	2D	0
Case 2 (offset case)	2D	0.5D

*D = 126m is the diameter of the rotor.

Computation Domain and Boundary Condition

All cases adopt the same computation domain. The length and width of computation domain are 5λ and 2λ (λ is wave length), respectively. Considering the expansion effect of turbine wake, the height of air phase is $2D$ (D = 126m is the diameter of the rotor). The depth of water phase is set to be 70% of the real water depth (d = 320m), for the effect of the water depth on the motion responses can be ignored at that water depth. The length of sponge layer before outlet boundary is 100m. The computational domain is shown in Fig. 7.

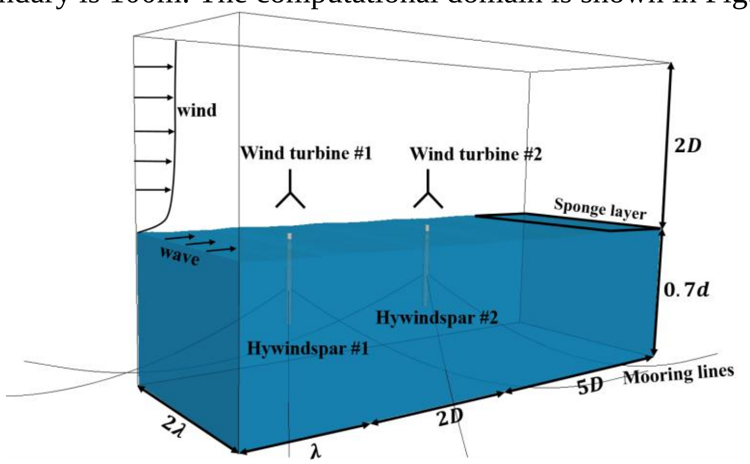

Fig. 7 Computational domain

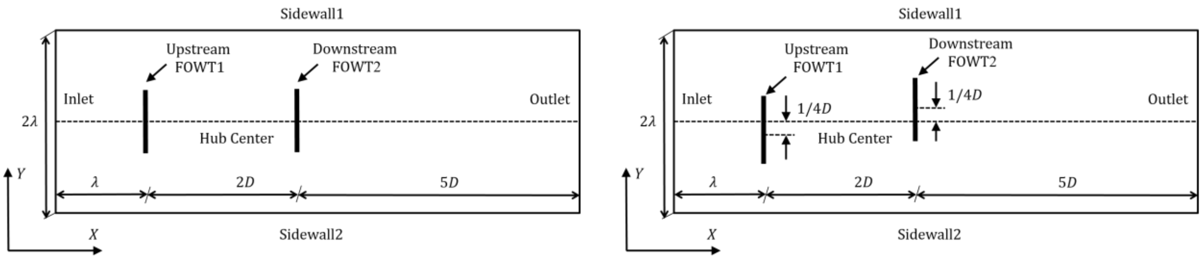

(*a*) Tandem configuration **(*b*) Offset configuration**

Fig. 8 Different arrangements of FOWTs

In these two cases, the distance from the inlet boundary to upstream FOWT is λ. The distance from the downstream FOWT to outlet boundary is 5*D*. For FOWTs in tandem case, the longitudinal distance between these two FOWTs is 2*D*, and the horizontal distance between two FOWTs is 0m. For FOWTs in offset case, the longitudinal distance between these two FOWTs is also 2*D*, while the horizontal distance between two FOWTs is 0.5*D*. Different arrangement of FOWTs in shown in Fig. 8.

To capture the wake flow of wind turbine, the refined girds are utilized in the region behind the wind turbine. And the grids near the water surface are refined to capture the free surface. The grid distribution is shown in Fig. 9

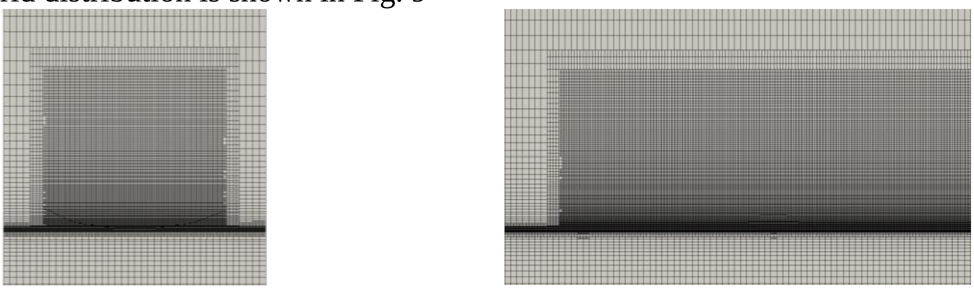

(*a*) Grid in lengthwise section **(*b*) Grid in cross section**

Fig. 9 Grid distribution

The boundary conditions are shown below:

(1) Inlet boundary: velocity condition is wave inlet condition, and pressure condition is Neumann boundary condition that the normal gradient of pressure is equal to zero;

(2) Outlet boundary: velocity condition is inletoutlet condition defined in OpenFOAM, and pressure condition is Dirichlet boundary condition that the pressure is constant;

(3) Top boundary: both velocity condition and pressure condition are Dirichlet boundary conditions;

(4) Bottom boundary: both velocity condition and pressure condition are slip conditions;

(5) Left boundary and right boundary: boundary conditions are defined as symmetry plane that directional derivative perpendicular to the boundary is equal to zero;

(6) Body surface: the moving wall boundary condition is adopted.

Results and Discussion

Aerodynamic Loads

Unsteady aerodynamic loads including the rotor power and thrust are presented here to analysis the influence of layout on the aerodynamic performance of FOWTs. The time history curves of rotor power and thrust of FOWTs in tandem and offset configurations are shown in Fig. 10 and Fig. 11, respectively.

The rotor power and thrust of FOWTs in two simulation cases both fluctuate greatly and change periodically, and the change period is approximately equal to the incident wave period. It indicates that this fluctuation and periodicity of the aerodynamic loads is in a large part due to the motions of floating support platform. The platform motions have significant effects on the unsteady aerodynamic performance of the FOWTs.

The time-averaged values of aerodynamic loads are listed in table 5. The rotor power and thrust of downstream FOWT are obviously smaller than those of upstream FOWT. In tandem case, the rotor power and thrust of downstream FOWT are only 30% and 62% compared to upstream FOWT. And the rotor power and the thrust of the downstream FOWTs are 78% and 85% compared to upstream FOWT in offset case, respectively. Due to the wake interaction between the FOWTs, the downstream FOWT experiences lower incoming wind velocity and higher turbulence intensity compared with the upstream FOWT, resulting in the aerodynamic loads decrease of downstream FOWT. It suggests the aerodynamic loads of downstream FOWT are affected significantly by the wake from upstream FOWT.

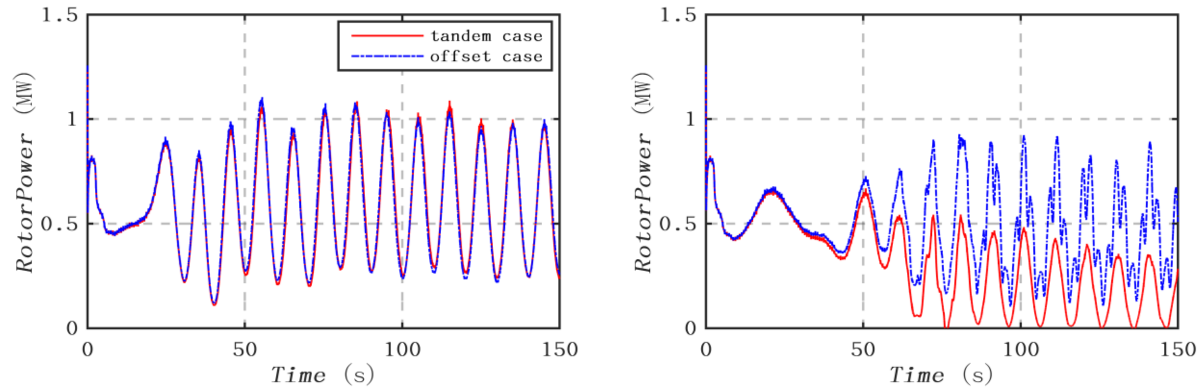

(*a*) Upstream wind turbine **(*b*) Downstream wind turbine**

Fig. 10 Time history curves of rotor power in tandem and offset configurations

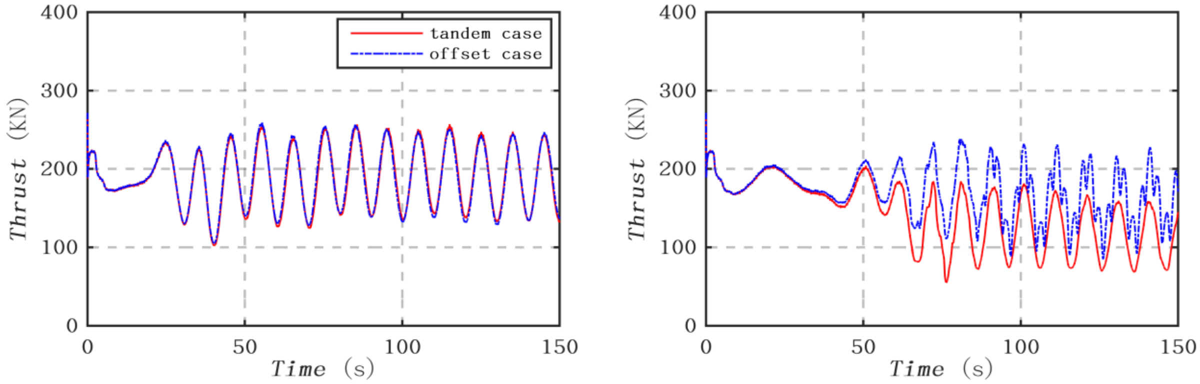

(*a*) Upstream wind turbine **(*b*) Downstream wind turbine**

Fig. 11 Time history curves of thrust in tandem and offset configurations

Table 5 Rotor power and thrust of FOWTs in tandem and offset configurations

		Power (kW)	Power ratio (*FOWT2/FOWT1*)	Thrust (kN)	Thrust ratio (*FOWT2/FOWT1*)
Case 1	FOWT 1	610	30%	193	62%
	FOWT 2	182		119	
Case 2	FOWT 1	588	78%	189	85%
	FOWT 2	459		161	

*FOWT 1 and FOWT 2 represent the upstream FOWT and downstream FOWT, respectively.

Table 6 Comparisons between aerodynamic loads in tandem and offset configurations

		Power (kW)	Power ratio (*Case1/Case2*)	Thrust (kN)	Thrust ratio (*Case1/Case2*)
FOWT 1	Case 1	610	96%	193	98%
	Case 2	588		189	
FOWT 2	Case 1	182	40%	119	74%
	Case 2	459		161	

The comparisons between rotor power and thrust in tandem and offset configurations are shown in table 6. For upstream FOWT, the time-average aerodynamic loads in tandem case are almost identical to those in offset case. And the aerodynamic loads of upstream FOWT in different layouts shown in Fig. 10(*a*) and Fig. 11(*a*) show little discrepancy. It means that the FOWT layouts have little effect on the aerodynamic loads of the upstream FOWT. While the situation is quite different for downstream FOWT. The time averaged value of the rotor power and thrust of downstream FOWT in tandem case are 40% and 74% compared to those in offset case. And notable discrepancy between the aerodynamic loads of downstream FOWT in tandem case and offset case can be found in Fig. 10(*b*) and Fig. 11(*b*). The variation progress of aerodynamic loads in offset case is more complex than that in tandem case. In tandem case, the downstream FOWT is in full wake, while the downstream FOWT is in half wake in offset case. So the average incoming wind velocity and turbulence intensity for downstream FOWT in offset case are larger than those in tandem case, which leads to the discrepancy in the aerodynamic loads of downstream FOWT in offset case and tandem case. It suggests that FOWT layouts have significant effects on the aerodynamic loads of the downstream FOWT.

Above all, it can be found that the aerodynamic loads are greatly influenced by the motions of floating support platform. The rotor power and thrust both fluctuate greatly and vary periodically. The aerodynamic loads of downstream FOWT are much smaller than those of upstream FOWT. The FOWT layouts have little influence on the aerodynamic loads of upstream FOWT, and the offset layout of the FOWTs have beneficial effects on the aerodynamic loads of downstream FOWT compared with the tandem layout.

Platform Motions

The floating support platform is an important part of the FOWT system. The platform motions have significant effects on the aerodynamic performance of wind turbine, and the aerodynamic forces will act on the floating platform and influence the motion responses in turn. There are complicated coupling effects between the floating support platform and wind turbine. The motion responses of floating support platforms in different layouts are shown in Fig. 12 and Fig. 13. The platform motions are compared and analyzed to investigate the influence of layouts on motion responses.

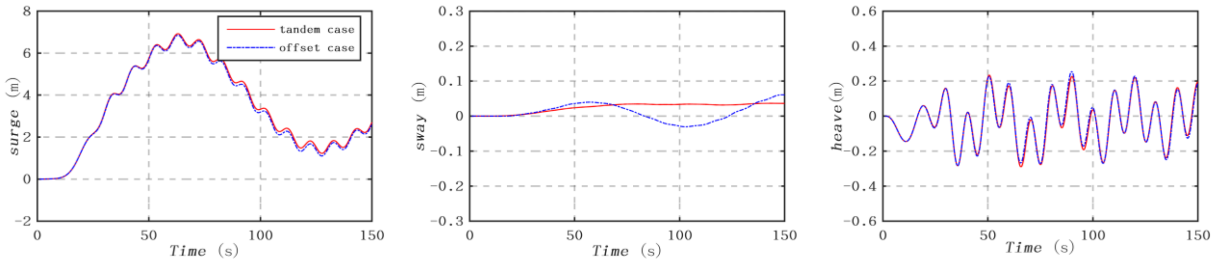

(*a*) Surge **(*b*) Sway** **(*c*) Heave**

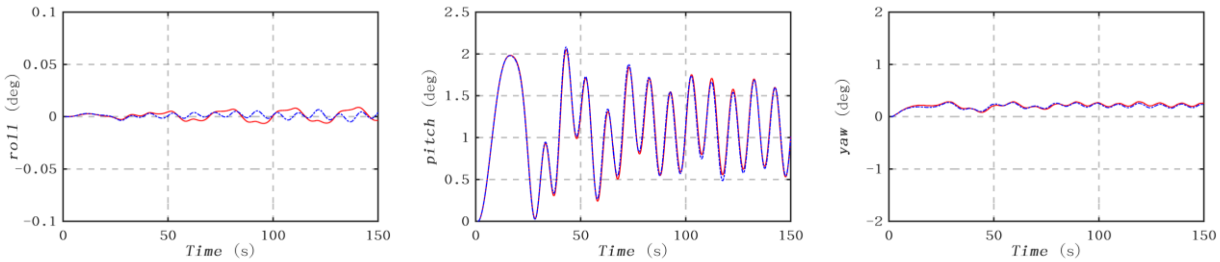

(*d*) Roll **(*e*) Pitch** **(*f*) Yaw**

Fig. 12 Motion responses of upstream platform in tandem and offset configurations

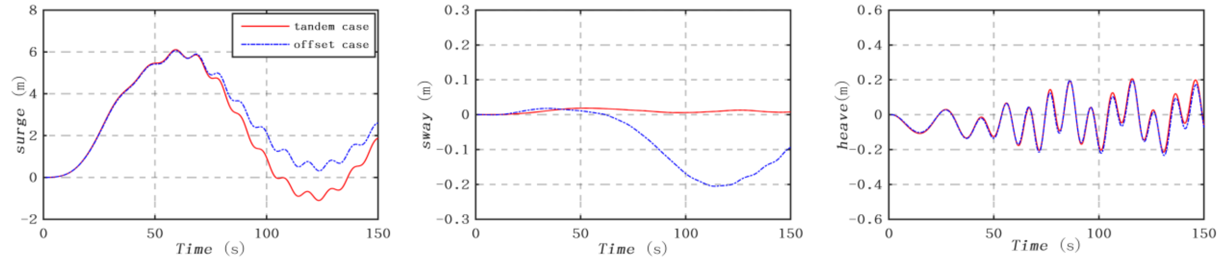

(*a*) Surge **(*b*) Sway** **(*c*) Heave**

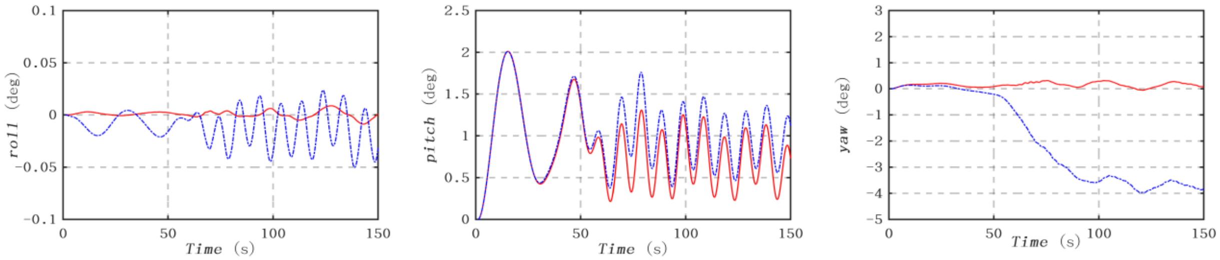

(*d*) Roll **(*e*) Pitch** **(*f*) Yaw**

Fig. 13 Motion responses of downstream platform in tandem and offset configurations

For the upstream platform, the six-degree-of-freedom motions in tandem case are much the same with the motions in offset case. It is because the loads acting on the upstream platform in different cases are almost identical. The loads acting on the floating support platform include the aerodynamic forces, wave loads and mooring forces. And these forces acting the upstream platform are nearly the same in different cases. It means the motion responses of the upstream platform have little difference in different FOWT layouts.

For the downstream platform, there is large difference between the motions in tandem and offset configurations. It can be seen that the average value of pitch motion of downstream platform in offset case is larger than that in tandem case. This large amplitude of pitch motion will lead to serious interaction between the rotor and its wake. As motioned above, the aerodynamic forces of downstream FOWT in offset case are larger than those in tandem case, and the aerodynamic forces will act on the floating support platform. It indicates the loads acting on the downstream platform in offset case are larger than those in tandem case, which explains the discrepancy of pitch motions of downstream platform between the tandem case and offset case. In addition, the amplitudes of sway and yaw motions of the downstream platform in tandem case are much larger than those in offset case. When the FOWTs is in offset configuration, the downstream FOWT is in half wake of the upstream FOWT. Affected by the wake interaction, the incoming wind velocity of the part of rotor in the wake are much larger than that not in the wake. This causes the forces acting on the rotor plane are not uniform. So the yaw and sway motions of the downstream platform in offset case are much larger than those in tandem case. For surge, roll and heave motions of the downstream platform, there is little discrepancy between the tandem case and the offset case.

Wake Field

The wake interaction between the FOWTs in both tandem and offset configurations are clearly observed. Detailed wake filed characteristics are presented here to study the wake interaction between two FOWTs in different layouts. Fig. 14 shows the contours of the axial direction wind velocity in the horizontal plane at the reference height z = 90m (the height of the center of rotor) for tandem case and offset case, respectively. The expansion of stream-tube is observed in both simulation cases. That the tangential velocity increases with decreasing axial direction wind velocity leads to this phenomena. In tandem case, the downstream FOWT is in full wake of the upstream FOWT. It can be seen the incoming wind velocity of the downstream FOWT decreases greatly compared with that of the upstream FOWT, which explains why the aerodynamic loads downstream FOWT are much smaller. In offset case, the downstream FOWT is in half wake of the upstream FOWT, so the incoming wind velocity of the part of downstream FOWT in the wake is smaller than that not in the wake. Furthermore, the asymmetric forces distributed on the rotor plane result in the yaw motion of the downstream FOWT. Compared with incoming wind velocity of the downstream FOWT in tandem case, the downstream FOWT in offset case experiences larger incoming wind velocity. So the aerodynamic loads of downstream FOWT in offset case are bigger than those in tandem case.

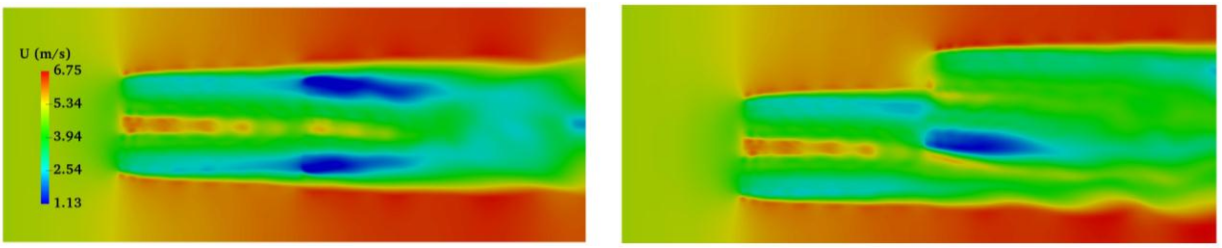

(*a*) Tandem configuration **(*b*) Offset configuration**

Fig. 14 Axial direction wind velocity counters in horizontal plane at the reference height z =90m

Profiles of the streamwise velocity in horizontal plane through the center of wind turbine rotor for different cases are presented in Fig. 15. The velocity profiles before the downstream FOWT in different cases are almost the same, while the velocity profile behind the downstream FOWT in offset case is quite different with that in tandem case. The velocity filed in offset case is more complicated, and the velocity deficit region in offset case is much larger.

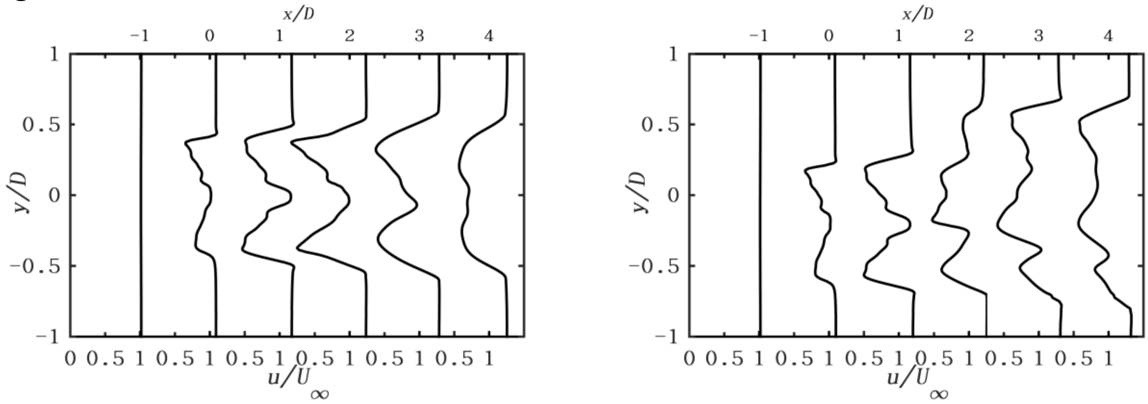

(*a*) Tandem configuration **(*b*) Offset configuration**

Fig. 15 Profiles of the streamwise velocity in horizontal plane through the center of wind

turbine rotor for different layouts

The evolution of wake vortex at different times of an entire wave circle in coupled case is illustrated in Fig. 16. The wave is contoured by wave height and the mooring lines are represented by black lines. The second-order invariant of velocity gradient tensor Q is used to visualize the wake vortex. Clearly spiral tip vortex from the upstream FOWT can be captured in both tandem and offset cases, while this vorticity is quickly diffused in the downstream. Affected by the wake of the upstream FOWT, the downstream FOWT experiences increased turbulence and the vortex structures become more unstable. In addition, the tip vortex from the downstream FOWT in tandem case are different from that in offset case. The tip vortex from downstream FOWT is much more affected by the wake of upstream FOWT in tandem case. Moreover, the platform motions lead to the interaction between the rotor and its wake and increase the instability of wake field.

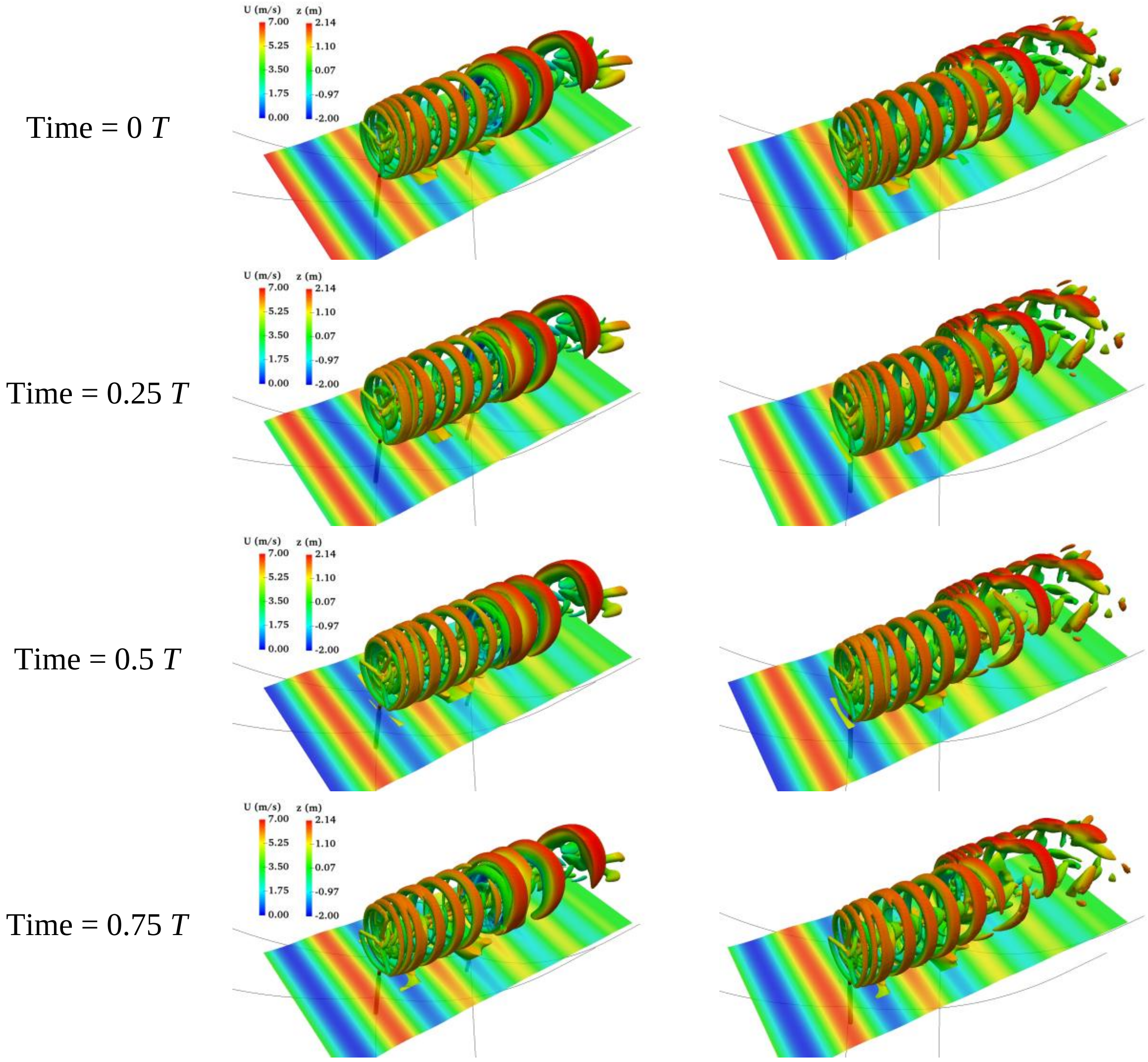

(*a*) **Tandem configuration** (*b*) **Offset configuration**

Fig. 16 Instantaneous vortex structure of the rotor in tandem and offset cases

Conclusions

In this study, the unsteady actuator line model (UALM) is embedded into in-house CFD solver naoe-FOAM-SJTU to establish a fully coupled CFD analysis tool named FOWT-UALM-SJTU for full-scale simulations of FOWTs. Coupled aero-hydrodynamic simulations of two OC3 Hywindspar FOWT models in both tandem and offset configurations under shear wind and regular wave conditions are performed. The aerodynamic loads including the rotor power and thrust, the six-degree-of-freedom motions and detailed wake field characteristics are obtained and analyzed. It can be found that aerodynamic loads are greatly influenced by the motions of floating support platform, which causes the rotor power and thrust both fluctuate greatly and change periodically. Affected by the wake interaction, the aerodynamic loads of downstream FOWT are much smaller than those of upstream FOWT. The FOWT layouts have little influence on the aerodynamic loads of upstream FOWT, and the offset configuration of the FOWTs have beneficial effects on the aerodynamic loads of downstream FOWT compared with the tandem configuration. For platform motions, the FOWT layouts have significant effects on the pitch, sway and yaw motions of downstream platform. While the surge, roll and heave motions are little influenced. The amplitudes of pitch, sway and yaw motions of downstream platform in offset configuration are much larger than those in tandem configuration. The wake field becomes more complicated affected by the wake interaction between the FOWTs. The tip vortex of upstream FOWT is clear, while the vortex structure of downstream FOWT is highly unstable. In addition, the wake characteristics of downstream FOWT in tandem configuration are much influenced the wake of upstream FOWT. In the future, the influence of inter-turbine spacing between FOWTs on wake field characteristics will be studied for the optimal layout design of floating wind farms.

Acknowledgement

This work is supported by the National Natural Science Foundation of China (51490675, 11432009, 51579145), Chang Jiang Scholars Program (T2014099), Shanghai Excellent Academic Leaders Program (17XD1402300), Program for Professor of Special Appointment (Eastern Scholar) at Shanghai Institutions of Higher Learning (2013022), Innovative Special Project of Numerical Tank of Ministry of Industry and Information Technology of China (2016-23/09) and Lloyd's Register Foundation for doctoral student, to which the authors are most grateful.

References

[1] Shen, X., Chen, J., Hu, P., Zhu, X., and Du, Z. (2018) Study of the unsteady aerodynamics of floating wind turbines, *Energy* 145, 793-809.

[2] Troldborg, N., Larsen, G. C., Madsen, H. A., Hansen, K. S., Sørensen, J. N., and Mikkelsen, R. (2011) Numerical simulations of wake interaction between two wind turbines at various inflow conditions, *Wind Energy* 14(7), 859–876.

[3] Bansal, J. C., Farswan, P., and Nagar, A. K. (2018) Design of wind farm layout with non-uniform turbines using fitness difference based BBO, *Engineering Applications of Artificial Intelligence* 71, 45-59.

[4] Wang, L., Tan, A., and Gu, Y. (2016) A novel control strategy approach to optimally design a wind farm layout, *Renewable Energy* 95, 10-21.

[5] Rehman, S., Ali, S. S., and Khan, S. A. (2017) Wind farm layout design using cuckoo search algorithms, *Applied Artificial Intelligence* 30(10), 899-922.

[6] Choi, N. J., Sang, H. N., Jeong, J. H., and Kim, K. C. (2014) CFD study on aerodynamic power output changes with inter-turbine spacing variation for a 6 mw offshore wind farm, *Energies* 7(11), 7483-7498.

[7] Choi, N. J., Sang, H. N., Jeong, J. H., and Kim, K. C. (2013) Numerical study on the horizontal axis turbines arrangement in a wind farm: effect of separation distance on the turbine aerodynamic power output, *Journal of Wind Engineering & Industrial Aerodynamics* 117(117), 11-17.

[8] Fletcher, T. M., and Brown, R. E. (2010) Simulation of wind turbine wake interaction using the vorticity transport model, *Wind Energy* 13(7), 587–602.

[9] Mikkelsen, R., Sørensen, J. N., Øye, Stig, and Troldborg, N. (2007) Analysis of power enhancement for a row of wind turbines using the actuator line technique, *Journal of Physics Conference Series* 75, 012044.

[10] Kusiak, A., and Song, Z. (2010) Design of wind farm layout for maximum wind energy capture, *Renewable Energy* 35(3), 685-694.

[11] Katic, I., Højstrup, J., and Jensen, N. O., A simple model for cluster efficiency, *Proceedings European Wind Energy Association Conference and Exhibition*, Rome, Italy, 1986, 407-409.
[12] Crespo, A., Manuel, F., and Hernández, J., Numerical modelling of wind turbine wakes, *Proceedings of the 1990 European Communication Wind Energy Conference*, Madrid, Spain, 1990, 166.
[13] Ainslie, J. F., Development of an eddy viscosity model for wind turbine wakes, *Proceedings 7th BWEA Wind Energy Conference*, Oxford, 1985, 61-66.
[14] Larsen, G. C., Højstrup, J., and Madsen, H. A., Wind fields in wakes, *Proceedings 1996 European Union Wind Energy Conference*, Göteborg, 1996, 764-768.
[15] Whale, J., Anderson, C. G., An experimental investigation of wind turbine wakes using particle image velocimetry, *1993 European Communication Wind Energy Conference and Exhibition*, Lübeck-Travemünde, Germany, 1993, 457.
[16] Vermeer, L. J., Sørensen, J. N., and Crespo, A. (2003) Wind turbine wake aerodynamics, *Progress in Aerospace Science* 39(6–7), 467-510.
[17] Churchfield, M., Sang Lee, John Michalakes, and Moriarty, P. (2012) A numerical study of the effects of atmospheric and wake turbulence on wind turbine dynamics, *Journal of Turbulence* 13(14), 1-32.
[18] Troldborg, N, Larsen, G. C., Madsen, H. A., Hansen, K. S., Sørensen, J. N., and Mikkelsen, R. (2011) Numerical simulations of wake interaction between two wind turbines at various inflow conditions, *Wind Energy* 14(7), 859-876.
[19] Dörenkämper, M., Witha, B., Steinfeld, G., Heinemann, D., and Kühn, M. (2015) The impact of stable atmospheric boundary layers on wind-turbine wakes within offshore wind farms, *Journal of Wind Engineering & Industrial Aerodynamics* 144, 146-153.
[20] Barthelmie, R. J., Pryor, S. C., Frandsen, S. T., Hansen, K. S., Schepers, J. G., and Rados, K., et al. (2010) Quantifying the impact of wind turbine wakes on power output at offshore wind farms, *Journal of Atmospheric & Oceanic Technology* 27(8), 1302-1317.
[21] Sorensen, J. N., and Shen, W. Z. (2002) Numerical modeling of wind turbine wakes, *Journal of Fluids Engineering* 124(2), 393.
[22] Sørensen, J. N., Shen, W. Z., and Munduate, X. (2015) Analysis of wake states by a full‐field actuator disc model, *Wind Energy* 1(2), 73-88.
[23] Jonkman, J., Butterfield, S., Musial, W., and Scott, G. (2009) Definition of a 5-mw reference wind turbine for offshore system development, *Office of Scientific & Technical Information Technical Reports*, 1–75.
[24] Jonkman, J., and Musial, W. (2010) Offshore code comparison collaboration (oc3) for IEA wind task 23 offshore wind technology and deployment, *Office of Scientific & Technical Information Technical Reports* 303, 275-3000.